

E15-2013-115

L. N. Bogdanova \*, D. L. Demin, V. V. Filchenkov

STUDY OF THE MECHANISM  
OF MUON CATALYZED  $t + t$  FUSION REACTION

Submitted to «Ядерная физика»

---

\* Institute for Theoretical and Experimental Physics, Moscow, Russia

Изучение механизма мюонного катализа реакции синтеза  $t + t$ 

Исследован механизм ядерной реакции  $t + t \rightarrow {}^4\text{He} + 2n + 11,33 \text{ МэВ}$  методом мюонного катализа. Рассчитана модель каскада реакций с  ${}^5\text{He}$  в качестве промежуточного состояния. Приняты во внимание как основное, так и первое возбужденные состояния  ${}^5\text{He}$ . Проведено сравнение спектра энергий нейтронов, измеренного в недавнем эксперименте, с расчетным спектром Монте-Карло. При изменении параметров реакции мы получили оптимальные значения для относительных весов основного и возбужденных состояний  ${}^5\text{He}$ , энергии возбуждения и ширины возбужденного состояния.

Работа выполнена в Лаборатории ядерных проблем им. В.П.Джелепова ОИЯИ.

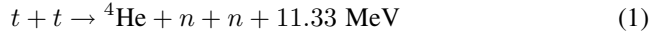
Study of the Mechanism of Muon Catalyzed  $t + t$  Fusion Reaction

The mechanism for the muon catalyzed fusion reaction  $t + t \rightarrow {}^4\text{He} + 2n + 11.33 \text{ MeV}$  is investigated. The model of the cascade reaction with  ${}^5\text{He}$  as an intermediate state is considered. Both the ground and the first excited states of  ${}^5\text{He}$  are taken into account. The neutron energy spectrum measured in the recent experiment is compared with the Monte Carlo-simulated one. Varying reaction parameters, we obtain optimum values for the relative weights of the  ${}^5\text{He}$  ground and excited states and for the excitation energy and width of the excited state.

The investigation has been performed at the Dzhelepov Laboratory of Nuclear Problems, JINR.

## 1. INTRODUCTION

Investigation of the muon catalyzed  $tt$  reaction



is of interest for the complete understanding of the muon catalyzed fusion ( $\mu\text{CF}$ ) processes in a hydrogen isotope mixture [1] and for the study of the nuclear reaction mechanism. The simplified scheme of  $\mu\text{CF}$  kinetics in tritium is shown in Fig. 1.

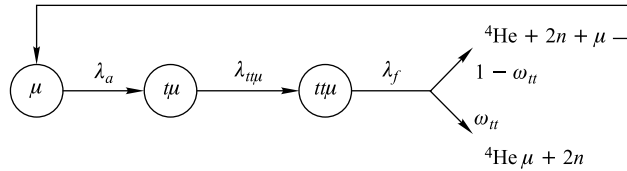


Fig. 1. Diagram of  $\mu\text{CF}$  kinetics in tritium

Stopping in tritium negative muons form  $\mu t$  atoms. Collisions of  $\mu t$  atoms with  $\text{T}_2$  molecules result in muonic molecules  $tt\mu$  nonresonantly produced in the rotational-vibrational state  $(Jv) = (11)$  at the rate  $\lambda_{tt\mu}$  [2]. Fusion reaction (1) competes with deexcitation of muonic molecules to the lower state  $Jv = (10)$  and with muon decay. The main deexcitation process is the  $E0$  Auger transition to the state  $Jv = (10)$  with the rate  $\lambda_{11 \rightarrow 10} = 2 \cdot 10^8 \text{ s}^{-1}$ . Deexcitation with the change of the total orbital angular momentum  $J$  (electric-dipole transitions) is considerably slower, its rate is  $\lambda_{\Delta J=1} < 10^5 \text{ s}^{-1}$  [3]. In fact, in muonic molecules with identical nuclei, due to relativistic effects these transitions require a change of the total nuclear spin. Since the rate of transitions with  $\Delta J = 1$  is smaller than the muon decay rate  $\lambda_0 = 4.6 \cdot 10^5 \text{ s}^{-1}$ , their role in muonic molecule deexcitation is negligible. Thus, a fusion reaction in the  $tt\mu$  molecule occurs from the  $p$ -wave state with a rate  $\lambda_f$ . After fusion, a muon either sticks to the helium nucleus with a probability  $\omega_{tt}$  or is released with a probability  $(1-\omega_{tt})$  and can catalyze a new fusion cycle.

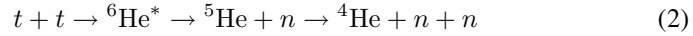
Fusion in the  $tt\mu$  molecule proceeds at very low energies ( $\sim 0.1 \text{ keV}$ ), which are hardly achievable in the beam-target experiments [4]. Till now the  $p$ -wave contribution to  $tt$  fusion cross section has not been determined in low-energy collision experiments due to a complicated analysis of the three-body final state [5]. In a  $\mu\text{CF}$  experiment one can deduce the  $p$ -wave reaction constant from the measured fusion rate  $\lambda_f$  [1]. In addition, spectra of fusion neutrons can be analyzed and give a unique possibility of studying the decay energy distribution among all three particles. Indications of the reaction mechanism are found through

**Table 1. Values of  $\omega_{tt}$  calculated in [6] under different assumptions of the reaction mechanism for the  $\mu\text{CF } tt$  reaction**

Interaction variant	Phase space	$n - n$ correlation	$\alpha - n$ correlation
$\omega_{tt}, \%$	10	5	18

this analysis. In addition, an extra constraint appears in  $\mu\text{CF}$  process. It is the muon sticking probability  $\omega_{tt}$  sensitive to the energy spectrum of  ${}^4\text{He}$  which reflects particle correlations in the three-body final state. The results of the  $\omega_{tt}$  calculations for different  $tt$  fusion schemes made in [6] are presented in Table 1.

Later calculations [7] considering the sequential model mechanism



give

$$\omega_{tt} = 14\%. \quad (3)$$

The main  $\mu\text{CF } t + t$  cycle parameters:  $\lambda_{tt\mu}$ ,  $\omega_{tt}$  and  $\lambda_f$  are obtained experimentally from the analysis of the neutron yields and time distributions in reaction (1). In this case, we have only two experimentally measured parameters (neutron time spectrum slopes). The third parameter, the absolute neutron yield  $Y_n^0$ , remains undetermined because of the unknown character of the neutron spectrum and therefore of the neutron detection efficiency  $\epsilon_n$ .

The solution to the problem was found in [8], where it was proposed to determine  $\omega_{tt}$  from the ratio

$$\eta_2/\eta_1^2 = 1 - \omega_{tt},$$

where  $\eta_1$  and  $\eta_2$  are the experimental yields of neutrons from the first and second  $\mu\text{CF}$  cycles. This method was used in [9] and [1]. It is important that the method is effective only for large efficiency  $\epsilon_n$ , which was obtained in the JINR experiment [1], where the unique full-absorption neutron spectrometer [10] was used. This allowed a twice better accuracy compared to [9], though a more intense muon beam was used there.

The results of three experiments on  $\mu\text{CF}$  in tritium [9] (PSI), [11] (RIKEN-RAL) and [1] (JINR) are presented in Table 2.

The neutron detector (ND) response (energy spectrum) was measured in those experiments too. All authors noted that the spectrum was appreciably harder than could be expected from the pure phase space distribution and interpreted this as an indication of the  $\alpha - n$  correlation in the final state of reaction (1).

**Table 2. Parameters of the  $\mu$ CF cycle measured in experiments**

Source of data	Ref.	$\lambda_{tt\mu}(10^6 \text{ s}^{-1})$	$\lambda_f(10^6 \text{ s}^{-1})$	$\omega_{tt}, \%$
PSI experiment	[9]	$1.8 \pm 0.6$	$15 \pm 2$	$14 \pm 3$
RIKEN-RAL experiment	[11]	$2.4 \pm 0.6$	no	$8.7 \pm 1.9$
JINR experiment	[1]	$2.84 \pm 0.32$	$15.6 \pm 2.0$	$13.9 \pm 1.5$

No serious attempts were made in [9, 11] and [1] to investigate the mechanism of reaction (1). The authors of [11] introduced two neutron energy groups as follows from reaction scheme (2)

$$E_{1n} = (6.25 \div 9.44) \text{ MeV}, \quad E_{2n} = (0.38 \div 5.08) \text{ MeV}. \quad (4)$$

The energies in the neutron groups were adjusted to obtain the best agreement of the ND response with experiment. Under these assumptions, the authors could, as is seen in Fig. 2, satisfactorily describe the measured energy spectrum (except its low-energy part) and estimate the neutron detection efficiency ( $\epsilon_n$ ), which was required for their analysis. However, parameters of process (2) were not obtained.

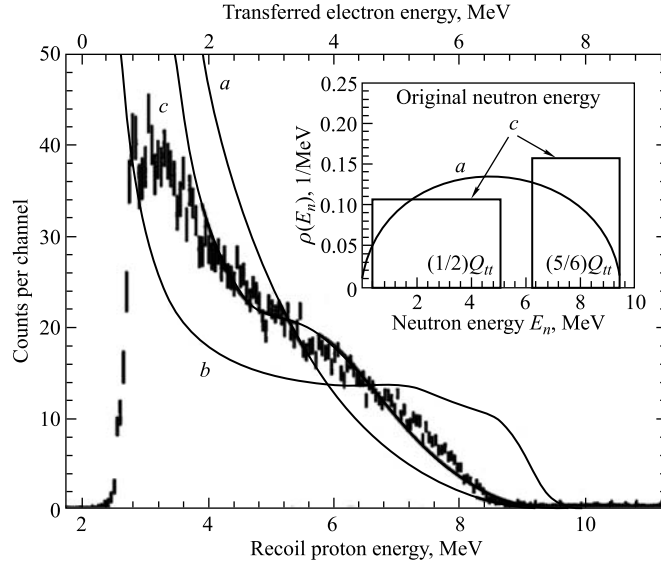


Fig. 2. Neutron detector (ND) response measured in [11]. Points are the experimental data, lines correspond to the calculations of the response under different assumptions on the neutron spectrum: *a*) phase space; *b*) strong  $\alpha - n$  correlations; *c*) neutron energy distribution (4)

Our model-independent analysis [1] makes it possible to check the reaction (1) mechanism. The aim of the present paper is as follows:

1) To obtain information on the reaction (1) mechanism by comparing the measured neutron energy spectrum (ND response)  $F(E_n)$  with the detailed Monte Carlo calculations.

2) To estimate  $\omega_{tt}$  using the simulated energy spectra of  $\alpha$  particles.

The agreement between the measured and calculated values would be beneficial both for increasing the experimental accuracy and for selecting the reaction mechanism.

## 2. EXPERIMENT

Our experiment on the study of the  $\mu$ CF process in tritium was completely described in [1]. Here we pay attention to the experimental geometry, specific features of the neutron detection system and some selection criteria for the neutron events. The experiment was performed at the TRITON setup mounted at the muon channel of the JINR Phasotron. The experimental setup is schematically shown in Fig. 3.

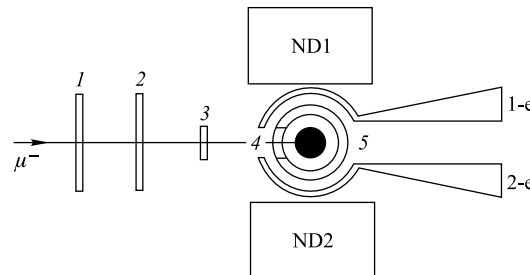


Fig. 3. Scheme of the experiment [1] on the investigation of the  $\mu$ CF process in tritium

Scintillation counters 1–3 detect incoming muons, which then stop in the liquid-tritium target (a black circle in Fig. 3). The target was 4 cm high and 1 cm in diameter. The tritium density was  $\phi = 5 \cdot 10^{22}$  n/cm<sup>3</sup>. The total thickness of the target copper ampoule and refrigerator walls (stainless steel) did not exceed 0.2 cm.

Proportional counters 4 and 5 detected muon stops in the target and electrons from the muon decay. Detectors 1-e and 2-e registered  $\mu$ -decay electrons in coincidence with counter 5. The scintillator thickness in each electron detector was 5 mm.

The full absorption neutron spectrometer [10] consisting of two large detectors (ND1 and ND2, each 11.5 l in volume), was the basis of the detection system. It detected neutrons from reaction (1). The cell of each detector was 310 mm in diameter and 150 mm high and filled with liquid scintillator NE-213. The scintillator properties allow the  $n - \gamma$  separation and discrimination of the relativistic background. The  $\gamma$ -quantum discrimination efficiency was better than  $10^{-3}$  for the gamma rays, whose electron energies are larger than 100 keV. The large size of the ND ensured a high neutron detection efficiency. The intrinsic detection efficiency for neutrons from the investigated process was close to 50%; the solid angle was 30% ( $0.3 \times 4\pi$  sr) for each ND.

The ND signals were scanned by the Flash ADC with a frequency of 100 MHz. Thus, each individual signal was a set of neighboring amplitudes which we call a cluster [12]. The sum of the amplitudes belonging to the same cluster is the cluster «charge». The detector response function is the distribution of the ND cluster charges. The measured response function is shown in Fig. 4 on the scale of the equivalent (to proton energy) electron energy  $E_{ee}$ . The charge calibration was done at the edge ( $E_n = 14.1$  MeV or  $E_{ee} \simeq 7.4$  MeV [10]) of the appropriate spectrum for the  $d + t$  fusion process which was also measured in the experiment [1]. The total ( $t + t$ ,  $d + t$ ) spectrum is shown in Fig. 4 without subtraction of the  $d + t$  fraction, which was few percent. Its shape is known from our previous experiments [13]. The subtracted spectrum was used for the analysis.

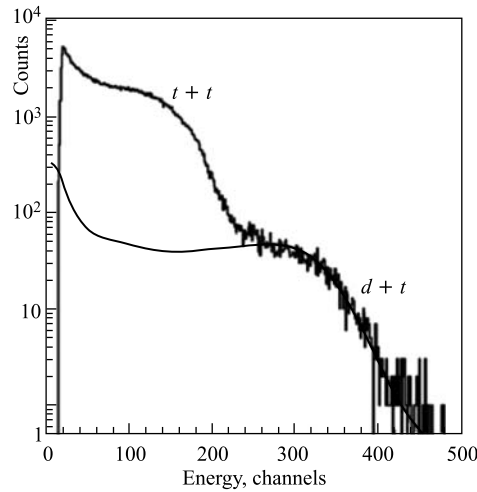


Fig. 4. Total ND charge spectrum measured in the experiment [1]

### 3. POSSIBLE VARIANTS OF THE ENERGY DISTRIBUTION AMONG THREE PARTICLES IN THE FINAL STATE OF THE FUSION REACTION IN THE $tt\mu$ MOLECULE

A possible region for the two neutron energies ( $E_{n1}, E_{n2}$ ) according to the kinematics of reaction (1) is shown in Fig. 5.

For the pure phase space variant of the energy distribution among three particles, the points are placed uniformly inside the contour limited by the lower line corresponding to the zero angle between the neutron directions and the upper one corresponding to the angle of  $180^\circ$ . The single-neutron energy distribution integrated over the phase space is presented in Fig. 6. Events corresponding to the  $n - n$  correlation are grouped around the point with equal neutron energies

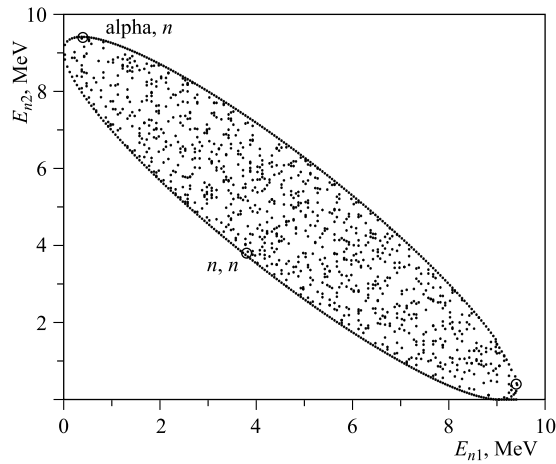


Fig. 5. The Dalitz plot for the pure phase space energy distribution

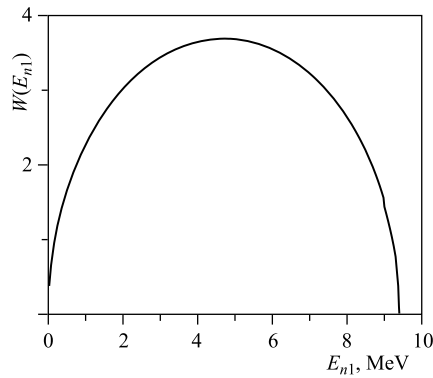


Fig. 6. Single-neutron energy spectrum for the pure phase space energy distribution

$E_{n1} = E_{n2} = 3.8$  MeV. The  $\alpha - n$  correlation results in two neutron groups of high and low energy.

In Fig. 7, we present our simulated spectra for the phase space (a) and for the scheme of  $t+t$  reaction via the sequential decay through  ${}^5\text{He}$  ground state (c) and the measured ND charge spectrum (b).

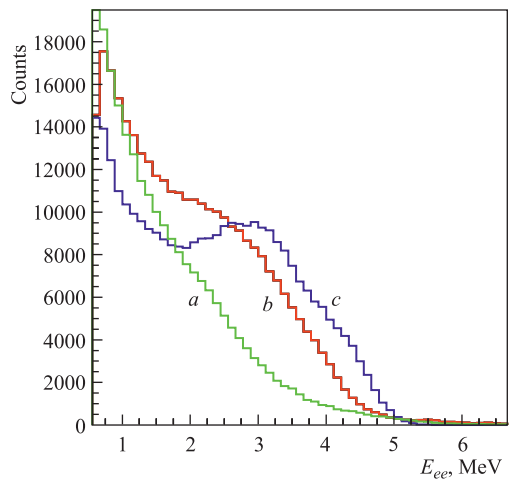


Fig. 7. ND charge spectrum measured in our experiment (b), the spectra simulated for the phase space (a) and  $\alpha - n$  correlations (only  ${}^5\text{He}$  ground state) (c)

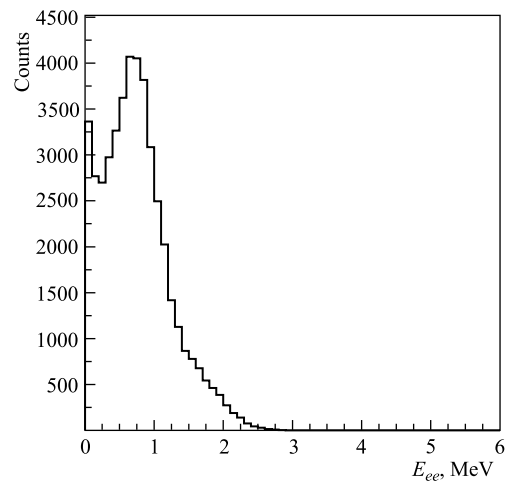


Fig. 8. ND charge spectrum simulated for the  $n - n$  correlated events of the  $t+t$  reaction

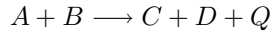
A comparison of the measured spectra from [11] (Fig. 2) and [1] reveals some similarity between them. They both are harder than in the phase space variant and softer than predicted for the  $\alpha - n$  correlation with the maximum possible neutron energies which are expected if one considers only the ground state of  ${}^5\text{He}$ .

The properties of our neutron spectrometer make the separation of the probable  $n - n$  correlation yield feasible. In Fig. 8, we present the ND response calculated for the case where the energy of each neutron was simulated around the value  $E_{n1,n2} = 3.8$  MeV with a small angle between them. One can see that the response is a full absorption peak around  $E_{ee} \simeq 1$  MeV. These features were not observed in the measured spectrum.

So we decided to consider the  $tt$  fusion reaction as a sequential process (2) taking into account the  ${}^5\text{He}$  ground and first excited states.

#### 4. SEQUENTIAL DECAY SCHEME FOR THE $t + t$ REACTION. ENERGY BALANCE

**4.1. Notations. Numerical Values.** The energy  $Q$  for the reaction



is expressed as a difference of masses ( $M$ ) of the particles participating in the reaction

$$Q = (M_A + M_B) - (M_C + M_D) - E^*(C) - E^*(D), \quad (5)$$

where  $E^*$  are the excitation energies of the outgoing particles. It is convenient to use masses  $m$  related to the  ${}^{12}\text{C}$  mass. The conversion to the absolute mass  $M$  is performed using the unit mass  $u$

$$M = m \cdot u, \quad u = 931.49432(28) \text{ MeV}.$$

The value of  $u$  is taken from [14].

A real calculation of  $Q$  involves the mass excess

$$\Delta M = (m - A) \cdot u,$$

where  $A$  is the atomic number of the nucleus. So, expression (5) takes the standard form

$$Q = (\Delta M_A + \Delta M_B) - (\Delta M_C + \Delta M_D) - E^*(C) - E^*(D). \quad (6)$$

The values of  $m$  and  $\Delta M$ , which were obtained using the data from [14, 15] and [16] are presented in Table 3.

**Table 3. Relative masses and mass excess for the nuclei participating in the investigated process**

Nucleus	Relative mass, $m$	Mass excess, $\Delta M$ (MeV)	Reference
$n$	1.008 664 91574(56)	8.0701	[12, 13]
$t$	3.016 049 2777(25)	14.929	[12, 13]
${}^4\text{He}$	4.002 603 254 143(63)	2.425	[12, 13]
${}^5\text{He}$	5.0120	11.294	[14]

**4.2. The First Stage of the Process under Study.** Here we consider the reaction

$$t + t \rightarrow {}^5\text{He} + n + Q_1. \quad (7)$$

Using the values from Table 1 and Eq. (6), we obtain

$$Q_1 = (10.534 - y) \text{ MeV}, \quad (8)$$

where  $y$  is the excitation energy of  ${}^5\text{He}$ . In fact, this value varied in accordance with the level width  $\Gamma$  (FWHM), which corresponds to the standard deviation  $\sigma = \Gamma/2.37$  of the Gaussian distribution.

According to [16], for the  ${}^5\text{He}(3/2^-)$  *ground state (GS)* we have

$$y_{\text{GS}} = 0; \quad \Gamma_{\text{GS}} = 0.648 \text{ MeV} \quad (\sigma_{\text{GS}} = 0.273 \text{ MeV}). \quad (9)$$

So, the neutron and  ${}^5\text{He}$  energies for the  ${}^5\text{He}$  ground state are

$$E_{1n} = 5/6 \cdot 10.534 = 8.778 \text{ MeV}, \quad E_{5\text{He}} = 1/6 \cdot 10.534 = 1.756 \text{ MeV}. \quad (10)$$

Since the level width is finite, these values should be treated as mean values for a Gaussian with the standard deviation  $\sigma_1 = 0.273 \text{ MeV}$ .

For the *first excited (EXS)* state of  ${}^5\text{He}(1/2^-)$  the parameters presented in [16] are

$$y_{\text{EXS}} = 1.27 \text{ MeV}, \quad \Gamma_{\text{EXS}} = 3.18 \text{ MeV} \quad (\sigma_{\text{EXS}} = 1.34 \text{ MeV}). \quad (11)$$

The corresponding neutron and  ${}^5\text{He}$  mean energies are

$$E_{1n} = 5/6 \cdot (10.534 - 1.27) = 7.738 \text{ MeV},$$

$$E_{5\text{He}} = 1/6 \cdot (10.534 - 1.27) = 1.545 \text{ MeV}.$$

Obviously, the neutron energy must not be larger than the maximum possible energy of process (1):  $E_n^{\text{max}} = 5/6 \cdot Q_0 \text{ MeV} = 9.44 \text{ MeV}$ , where  $Q_0 = 11.33 \text{ MeV}$  is the total energy for reaction (1). This leads to the limitation

$$y \leq 0.799 \text{ MeV}.$$

**4.3. The Second Stage of the Process.** We consider the second stage of the process, namely, the in-flight decay of  ${}^5\text{He}$



in its center-of-mass system (CMS) and then go over to the laboratory system (LABS). According to the previous consideration, the reaction energy for process (12) is

$$Q_2 = (0.798 + y) \text{ MeV}. \quad (13)$$

In the CMS, this energy is distributed between the neutron and the  $\alpha$  particle ( $E_{n0} = 4/5 \cdot Q_2$ ,  $E_{\alpha0} = 1/5 \cdot Q_2$ ), which are emitted with the velocities  $v_{0n}$  and  $v_{0\alpha}$  in the opposite directions.

According to the kinematic rules, the energies of the outgoing particles in LABS are

$$E_x = m_x/2 \cdot (V^2 + v_{0x}^2 + 2 \cdot V \cdot v_{0x} \cdot \cos \theta_0), \quad (14)$$

with the bounds

$$E_{x,\min} = m_x \cdot (v_{0x} - V)^2/2, \quad E_{x,\max} = m_x \cdot (v_{0x} + V)^2/2. \quad (15)$$

In equations (14) and (15),  $m_x$  and  $v_{0x}$  are the masses of the neutron or the  $\alpha$  and their velocities in the CMS;  $\theta_0$  is the decay angle in the LABS and  $V$  is the  ${}^5\text{He}$  velocity which it acquired in process (7).

Here are some calculated values for the GS variant ( $y = 0$ ):

$$V = 2.74 \cdot 10^{-2}, \quad v_{0n} = 3,69 \cdot 10^{-2}, \quad E_{n,\min} = 0.42 \text{ MeV}, \quad E_{n,\max} = 1.94 \text{ MeV}.$$

Velocities are expressed in units of the speed of light. Similarly, for the EXC ( $y = 1.27$ ) we have

$$V = 2.57 \cdot 10^{-2}, \quad v_{0n} = 5.93 \cdot 10^{-2}, \quad E_{n,\min} = 0.37 \text{ MeV}, \quad E_{n,\max} = 2.97 \text{ MeV}.$$

For an isotropic angular distribution  $f(\theta_0)$  in the CMS, the energy distribution in the LABS should be uniform with the bounds (15) (with some distortions caused by the finite level width). Indeed, the distribution  $f(\theta_0)$  is anisotropic. Since  ${}^5\text{He}$  is formed in states of negative parity decaying in neutron and  $\alpha$ , the angular momentum and parity conservation require a correlation between the direction of the  ${}^5\text{He}$  motion and the subsequent direction taken by the neutron (alpha) it emits. The correlation function in the CMS is [17]

$$f(\theta_0) = 1 + 3 \cdot \cos^2 \theta_0. \quad (16)$$

The neutron energy spectra simulated for the GS case with parameters (9) and for the EXS state with  $y = \sigma = 1 \text{ MeV}$  are shown in Fig. 9 for the isotropic  $f(\theta_0)$  (as an illustration) and for real angular distribution (16).

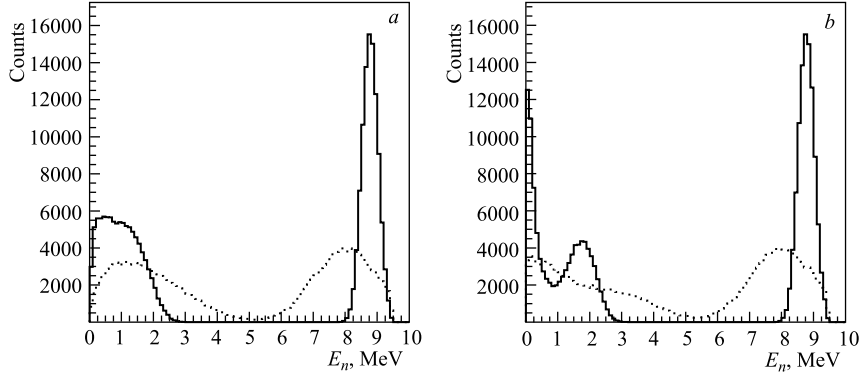


Fig. 9. Neutron energy spectra simulated for the GS case with parameters (9) (solid line) and for the EXS state with  $y = \sigma = 1$  MeV (dashed line). *a*) Isotropic angular distribution in the CMS; *b*) real distribution (16)

A comparison of Figs. 2 and 9 (left) shows that two groups of neutron energies chosen as an optimum in [11] and calculated by us for the  $^5\text{He}$  excited state are close to each other. It may attest to the dominant role of this state. On the other hand, the use of the isotropic angular distribution instead of (16) for the second neutrons in [11] leads to some impairing of the soft part of the detector response due to the threshold factor. It possibly explains the disagreement between the calculated and measured spectra in [11].

## 5. CALCULATIONS OF THE ND RESPONSE. COMPARISON WITH EXPERIMENT

**5.1. General Scheme.** The aim of calculations was to create the ND charge spectrum and find the optimum parameters describing reaction (2). Both the ground and the first excited states of  $^5\text{He}$  were taken into account. The parameters of the GS state were fixed according to (9) [16]. The energy and width of the excited state as well as the relative yields of these states  $\eta_{\text{GS}}$  and  $\eta_{\text{EXS}} = 1 - \eta_{\text{GS}}$  were variable parameters.

The calculations were performed with the Neutreff code [18], which was successfully used in our experimental program for the  $\mu\text{CF}$  investigations and checked using the independent code based on GEANT-4 [13]. The calculations were performed on the event-by-event basis until the required statistics was accumulated. For each event, the history of the first neutron (7) and the second neutron (12) was examined. The neutron charge was obtained by its calibration in  $E_{ee}$  units for the light output  $L(E_p)$  of the recoil protons from the  $n - p$

interaction in the ND scintillator. To obtain the  $E_{ee}(E_p)$  data we used the parameterization of the most accurate modern values from [19] which agree well with our measurements [10]. The accuracy of the parameterization was not worse than  $(2 \div 3)\%$ . The ND charge calibration was made using the edge of the spectrum corresponding to the registration of the  $d + t$  process (Fig. 4).

The neutron interactions in the «intermediate» matter (tritium in the target and plastic scintillator of detectors 1-e or 2-e) were taken into consideration. This leads to a change in the neutron energy and direction. The differential and total cross sections for the  $n - t$  interaction were taken from [20].

We checked whether the neutron came into one of the neutron detectors after leaving the plastic scintillator. If it did, then  $n - C$  and  $n - p$  interactions were considered. The data for the  $n - p$  and  $n - C$  cross sections were taken from [21, 22]. For  $(n, \gamma)$  interactions on carbon the fate of the gamma ray was examined. If it was registered in the ND, the corresponding event was excluded from the consideration.

After the required statistics was collected, the spectra from ND1 and ND2 were summed. This total spectrum was compared with the measured one. The errors in the experimental distribution are really only statistical. Systematic errors in the calculations mainly result from ambiguities in the approximations of the neutron cross sections and from the energy dependence of the light output. The maximum estimate of these errors is  $\simeq 3\%$ .

**5.2. Check of the Simulations with the Independent Calculations.** To check our code, we compared our results for an arbitrary variant ( $y = 0.8$  MeV,  $\sigma = 0.3$  MeV) with the results obtained by V. Bom [23] with the code based on

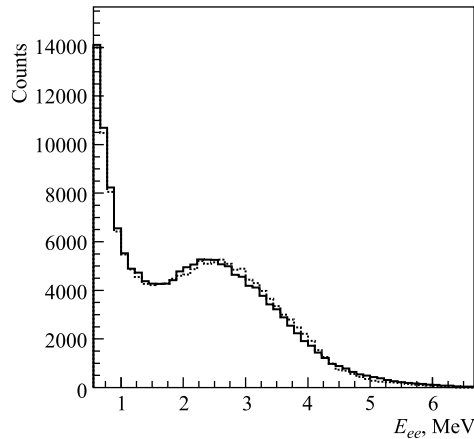


Fig. 10. ND charge spectra calculated for an arbitrary variant by V. Bom (full histogram) and in this paper (dashed histogram)

GEANT-4. Both calculations were compared for the conditions without a threshold to increase sensitivity to the calculation details. The corresponding spectra are shown in Fig. 10.

The detection efficiency for the total  $N_{\text{tot}}$  (ND1 and ND2) and coincidence  $N_{\text{coin}}$  (both detectors simultaneously) events are presented in Table 4.

**Table 4. Neutron detection efficiency calculated for an arbitrary variant in this work and by V. Bom with GEANT-4**

	Single events	Coincidence events
V. Bom	0.532	0.227
This work	0.530	0.229

Rather good agreement is seen between two independent calculations. Note that the detection efficiency sharply depends on the threshold.

For the real value  $E_{ee} = 0.5$  MeV,  $N_{\text{tot}} = 0.215$  and  $N_{\text{coin}} = 0.077$ .

**5.3. Optimization of the Parameters. The Main Results.** The procedure for the optimization of the parameters was as follows. It is seen in Fig.7 that the GS as the only «pure» variant cannot describe the measured spectrum. At the same time, the corresponding spectrum has distinctions as compared with the EXS. It allows  $\eta_{\text{GS}}$  to be found in the first approximation by using (9) and (11) as the initial parameters [16]. With this value, we could optimize the parameters for the EXS. It was a suitable way guided by the influence of  $y_{\text{EXC}}$  and  $\Gamma_{\text{EXS}}$  on the spectrum shape. Then, the appropriate value of  $\eta_{\text{GS}}$  was introduced, and the process was repeated until the best agreement was obtained. The agreement criterion was  $\chi^2$ .

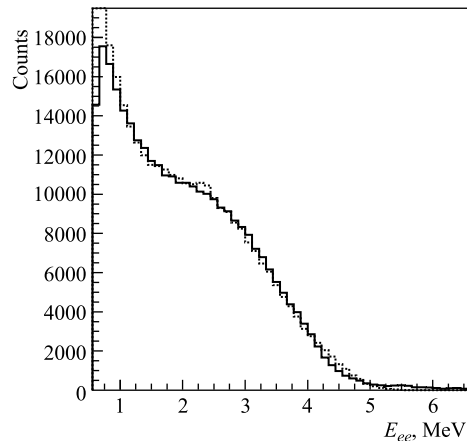


Fig. 11. The measured charge spectrum (full histogram) in comparison with the spectrum calculated with parameters (9) and (17) (dashed histogram)

The uncertainties in the investigated parameters were estimated in the three-dimensional region  $[\eta_{\text{GS}}, y_{\text{EXC}}, \Gamma_{\text{EXC}}]$ , inside which  $\chi^2$  varied by no more than a few units relative to its optimum value. The optimum value for the interval  $(8 \div 48)$  channels is  $\chi^2 = 48$ . It should mean a satisfactory result for the multiparameter Monte Carlo problem. The obtained results are

$$\eta_{\text{GS}} = (23 \pm 4)\%, \quad y_{\text{EXS}} = (1.02 \pm 0.16) \text{ MeV}, \quad \Gamma_{\text{EXS}} = (2.84 \pm 0.47) \text{ MeV}. \quad (17)$$

The ND response calculated for the fixed parameters (9) and found from our analysis (17) is presented in Fig. 11 in comparison with the measured one.

**5.4. Discussion.** As follows from our consideration, we succeeded in describing the energy distribution of neutrons from the  $t + t$  fusion reaction in a  $tt\mu$  molecule on the basis of sequential scheme (2). Comparing our results with the spectra expected for the pure phase space and the  $n - n$  correlation, we conclude that the partial yield for each of them does not exceed  $3 \div 5\%$ .

Let us now compare our results (17) for  ${}^5\text{He}$  EXC parameters with the modern data (11). One can see that our value for  $y_{\text{EXS}}$  differs from (11) by 1.5 standard deviations. For the level width the agreement is better: 1 standard deviation.

## 6. MUON STICKING TO ${}^4\text{He}$

The self-consistency of our description can be checked using one more observable in reaction (1) — muon sticking to  ${}^4\text{He}$ ,  $\omega_{tt}$ , measured in the experiment. The first estimations of  $\omega_{tt}$  made in [6] show that this value strongly depends

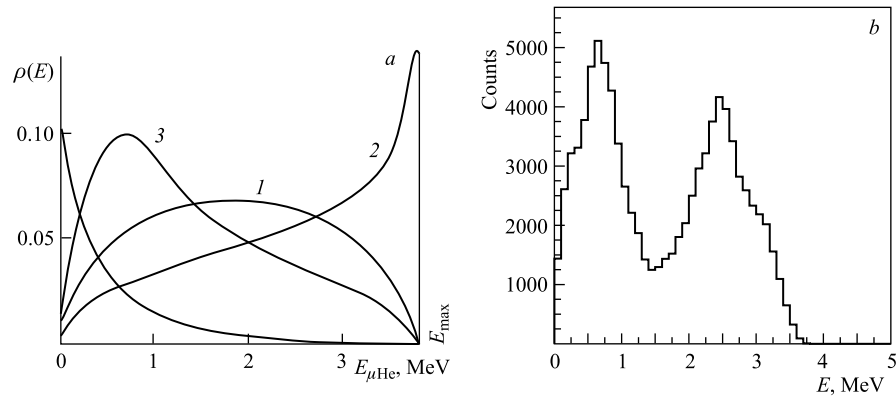


Fig. 12. *a*) Calculations made in [6] for the  $\mu\alpha$ -atom energy spectrum  $F(E_\alpha)$  produced in the  $tt$  reaction: 1 — statistical distribution, 2 —  $n - n$  correlation, 3 —  $n - {}^4\text{He}$  correlation, and dependence  $w_{tt}(E_\alpha)$ . *b*) The  $F(E_\alpha)$  spectrum simulated in this work

on the  $\alpha$ -particle spectrum, i. e., on the reaction (1) mechanism. This is illustrated in Fig. 12 (left) taken from that paper. In this figure (right), we present the  $\alpha$ -particle energy spectrum calculated on the basis of sequential mechanism (2) with parameters (11) and (17).

Detailed calculations of the sticking probability using the  $\alpha$  spectrum obtained in this work were performed with the probability densities of the initial sticking calculated by Markushin [26] as functions of the muonic helium initial velocity. The results are

$$\omega_{tt}^{1S} = 13.0\%, \quad \omega_{tt}^{\text{all}} = 15.9\%. \quad (18)$$

In order to compare the sticking probability calculated using the reconstructed  $\alpha$  spectrum with the experimental value we need to introduce correction for the muon stripping. Using estimation [26] we obtain  $\omega_{tt} = 14.4\%$ . Our experimental value is  $\omega_{tt}^{\text{exp}} = (13.9 \pm 1.5)\%$  [1]. It is good evidence for the self-consistency of our analysis.

## 7. CONCLUSION

The mechanism of reaction (1) from the  $tt\mu$ -molecule state was investigated for the first time. We analyzed the measured neutron energy (charge of the ND) spectrum  $F(E_n)$  using the Monte Carlo simulation of process (1). Guided by the neutron spectrum peculiarities and kinematics we chose for our calculations a scheme with the  ${}^5\text{He}$  ground and first excited states as intermediate ones. Sequential three-body decay proceeds via spatially confined quasi-stationary two-body configurations. Then two particles stay close to each other while the third one moves away. We succeeded in describing the measured spectrum  $F(E_n)$  with this phenomenological model and were able

- to determine the relative part of the ground and the first excited states of  ${}^5\text{He}$ ;
- to estimate independently the excitation energy and width of the  ${}^5\text{He}$  excited state (for the fixed parameters of the ground state);
- to determine the  $\alpha$ -particle energy spectrum. The reconstructed  $\alpha$  spectrum was used for calculating the muon sticking probability  $\omega_{tt}$ , which depends on the energy distribution among three particles in the final state of the  $tt$  fusion reaction.

Of course, the most sensitive test of the mechanism for the  $t+t$  reaction from the  $p$ -state of  $tt\mu$  would be direct measurement of the  $\alpha$ -particle energy spectrum using a thin solid layer of tritium in vacuum. Similar investigations (for other  $\mu\text{CF}$  processes) were performed at TRIUMF [27].

It is tempting to relate the mechanism of the  $tt$  reaction «at rest», as in the  $tt\mu$  molecule, to a more general problem of the  ${}^6\text{He}$  nucleus spectroscopy. The known spectrum of  ${}^6\text{He}$  contains the  $0^+$  bound state, the well-known  $2^+(E^* = 1.8 \text{ MeV})$

three-body resonance, and a desert in the three-body  $\alpha + n + n$  continuum up to the  $t + t$  threshold at about 13 MeV. This nucleus is known to have an excited state close to the  $t + t$  threshold ( $E_x = 14.6 \pm 0.7$  MeV,  $\Gamma = 7.4 \pm 1$  MeV) with the likely spin-parity  $1^-$  [16]. Since we deal with the three-body  $\alpha + n + n$  continuum close to the  $t + t$  threshold, we access the region of  ${}^6\text{He}$  excited  $1^-$  state. The three-body continuum properties are less known, although rather much studied over many years.

Some authors note that the most intriguing manifestations of clustering are the Borromean two-neutron halo nuclei ( ${}^6\text{He}$ ,  ${}^{11}\text{Li}$ ), in which the two-body subsystems are unbound. This behavior naturally gives rise to the question of the correlations between the constituents of these three-body systems. What are the specific features of the continuum of a system with a halo ground state? The recent developments in radioactive nuclear beam techniques and dynamic approaches to the three-body continuum theory make it possible to find out to what extent our knowledge of the lightest Borromean halo nucleus  ${}^6\text{He}$  is complete [28].

**Acknowledgements.** The authors are grateful to G.M.Ter-Akopyan and V.B.Belyaev for useful discussions. L.N.Bogdanova acknowledges the support by Grant NSh-3172.2012.2. The work was supported by the Russian Foundation for Basic Research, project No. 12-02-00089.

## REFERENCES

1. Bogdanova L.N. et al. // ZhETF. 2009. V. 135. P. 242; [JETP. 2009. V. 108. P. 215].
2. Ponomarev L.I., Faifman M.P. // ZhETF. 1976. V. 71. P. 1689; [Sov. Phys. JETP. 1976. V. 44. P. 886].
3. Vinitstil S.I., Ponomarev L.I., Faifman M.P. // ZhETF. 1982. V. 82. P. 985; [Sov. Phys. JETP. 1982. V. 55. P. 985].
4. Bogdanova L.N., Filchenkov V.V. // Hyp. Int. 2001. V. 138. P. 321.
5. Serov V.I., Abramovich S.N., Morkin L.A. // At. En. 1977. V. 42. P. 59; Agnew H.M. et al. // Phys. Rev. 1952. V. 84. P. 862.
6. Gershtein S.S. et al. // Sov. Phys. JETP. 1981. V. 53. P. 872.
7. Bogdanova L.N. // Muon Cat. Fusion. 1988. V. 3. P. 359.
8. Filchenkov V.V., Somov L.N., Zinov V.G. // Nucl. Instr. Meth. 1984. V. 228. P. 174; Filchenkov V.V. et al. JINR Preprint P15-82-566. Dubna, 1982.
9. Breunlich W.H. et al. // Muon Cat. Fusion. 1987. V. 1. P. 121.
10. Dzhelepov V.P. et al. // Nucl. Instr. Meth. A. 1988. V. 269. P. 634; Konin A.D., Rudenko A.I., Filchenkov V.V. // Nucl. Instr. Meth. A. 1990. V. 294. P. 504; Baranov V.A. et al. // Nucl. Instr. Meth. A. 1996. V. 374. P. 335; Filchenkov V.V. // PEPAN. 2003. V. 34. P. 1062.

11. *Matsuzaki T. et al. // Hyp. Int. 1999. V. 118. P. 229;*  
*Matsuzaki T. et al. // Hyp. Int. 2001. V. 138. P. 295;*  
*Matsuzaki T. et al. // Phys. Lett. B. 2003. V. 557. P. 176.*
12. *Filchenkov V. V., Drebusko A. E., Rudenko A. I. // Nucl. Instr. Meth. A. 1997. V. 395. P. 237.*
13. *Bom V. R. et al. // Hyp. Int. 1998. V. 118. P. 111;*  
*Bom V. R., Filchenkov V. V. // Hyp. Int. 1999. V. 119. P. 365.*
14. *Mohr P. J., Taylor B. N., Newell D. B. // Rev. Mod. Phys. 2008. V. 80. P. 633.*
15. *Karshenboim S. G. // Uspekhi Fiz. Nauk. 2005. V. 175. P. 271; [Phys. Usp. 2005. V. 48. P. 255].*
16. *Tilley D. R. et al. // Nucl. Phys. 2002. V. 708. P. 3.*
17. *Bams S. J. et al. // Phys. Rev. 1957. V. 106. P. 1237.*
18. *Filchenkov V. V., Marczis L. JINR Commun. E13-88-566. Dubna, 1988.*
19. *Naqvi A. A. et al. // Nucl. Instr. Meth. A. 1993. V. 325. P. 574.*
20. *Seagrave J. D. et al. // Phys. Rev. 1960. V. 119. P. 1981.*
21. *Del Guerra. A. // Nucl. Instr. Meth. 1976. V. 135. P. 337.*
22. T2 Nuclear Information Service: [t2.lanl.gov/data](http://t2.lanl.gov/data).
23. *Bom V. R. Private Communication.*
24. *Anghinolfi M. et al. // Nucl. Instr. Meth. 1979. V. 165. P. 217.*
25. *Benveniste J. et al. // Nucl. Phys. 1960. V. 19. P. 448;*  
*Fisher G. E. // Phys. Rev. 1954. V. 96. P. 704.*
26. *Markushin V. E. // Muon Cat. Fusion. 1988. V. 3. P. 395.*
27. *Marshall G. M. et al. // Hyp. Int. 1993. V. 82. P. 529.*
28. *Chulkov L. V. et al. // Nucl. Phys. A. 2005. V. 759. P. 23.*

Received on November 12, 2013.

Корректор *Т. Е. Попеко*

Подписано в печать 05.02.2014.

Формат 60 × 90/16. Бумага офсетная. Печать офсетная.

Усл. печ. л. 1,25. Уч.-изд. л. 1,68. Тираж 225 экз. Заказ № 58179.

Издательский отдел Объединенного института ядерных исследований  
141980, г. Дубна, Московская обл., ул. Жолио-Кюри, 6.

E-mail: [publish@jinr.ru](mailto:publish@jinr.ru)

[www.jinr.ru/publish/](http://www.jinr.ru/publish/)